

Demonstration of Tokamak Discharge Shutdown with Shell Pellet Payload Impurity Dispersal

E. M. Hollmann,¹ P. B. Parks,² D. Shiraki,³ N. Alexander,² N. W. Eidietis,² C. J. Lasnier,⁴ and R. A. Moyer¹

¹University of California–San Diego, La Jolla, California 92093, USA

²General Atomics, San Diego, California 92186, USA

³Oak Ridge National Laboratory, Oak Ridge, Tennessee 37831, USA

⁴Lawrence Livermore National Laboratory, Livermore, California 94550, USA



(Received 11 December 2018; published 12 February 2019)

The first rapid tokamak discharge shutdown using dispersive core payload deposition with shell pellets has been achieved in the DIII-D tokamak. Shell pellets are being investigated as a possible new path toward achieving tokamak disruption mitigation with both low conducted wall heat loads and slow current quench. Conventional disruption mitigation injects radiating impurities into the outer edge of the tokamak plasma, which tends to result in poor impurity assimilation and creates a strong edge cooling and outward heat flow, thus requiring undesirable high- Z impurities to achieve low conducted heat loads. The shell pellet technique aims to produce a hollow temperature profile by using a thin, low-ablation shell surrounding a dispersive payload, giving a greatly increased impurity ablation (and radiation) rate when the payload is released in the plasma core. This principle was demonstrated successfully using 3.6 mm outer diameter, 40 μm thickness diamond shells holding boron powder. The pellets caused rapid (<10 ms) discharge shutdown with low conducted divertor heat fluence (~ 0.1 MJ/m²). Confirmation of massive release of the boron powder payload into the plasma core was obtained spectroscopically. Some evidence for the formation of a hollow temperature profile during the shutdown was observed. These first results open a new avenue for disruption mitigation research, hopefully enabling development of highly effective methods of avoiding disruption wall damage in future reactor-scale tokamaks.

DOI: [10.1103/PhysRevLett.122.065001](https://doi.org/10.1103/PhysRevLett.122.065001)

Introduction.—Material ablation plays a crucial role in many fields, including ultraviolet light sources [1], planetary science [2], astrophysics [3], and medicine [4]. In the area of magnetic fusion energy research, detailed studies of material ablation in plasmas could help design methods to prevent costly wall damage from major disruptions in future tokamak-based powerplants. Major disruptions are global tokamak plasma instabilities, which can result from control system failure or from crossing stability boundaries. Although extensive research has been devoted to avoiding disruptions [5,6], it is doubtful that they can be avoided with 100% certainty, motivating the study of rapid shutdown methods to safely dissipate plasma energy in the event of an unavoidable disruption [7,8].

All rapid shutdown methods being studied involve the injection of impurities to radiate away the plasma energy. Several impurity delivery methods have been studied, including gas injection, cryogenic pellet injection (PI), and shattered cryogenic pellet injection (SPI) [9]. Good progress has been made in understanding tokamak rapid shutdowns, with shattered neon pellet injection presently considered the most promising method for rapid shutdown of the ITER tokamak [10].

Despite the progress made on rapid shutdown research, shortcomings persist in the present methods, partially

due to poor impurity assimilation resulting from edge deposition. Simultaneous reduction of induced vessel forces, conducted heat loads, and runaway electrons is challenging: higher- Z impurity injection tends to improve radiation efficiency, thus reducing conducted heat loads, but also causes more rapid electron temperature collapse (TQ) and more rapid current decay (CQ), thus increasing runaway electron (RE) production and induced vessel forces [9].

The dispersive shell pellet (DSP) concept seeks to increase impurity assimilation via the rapid delivery of a dispersive payload to the core of the discharge. High pressure gas [11] and dust [12] have been considered as payloads. An outer shell is used to hold the payload together and protect it from ablation at the plasma edge. In the ideal DSP shutdown, the pellet reaches the plasma core with minimal perturbation to the plasma, then releasing its payload and causing an inside-out TQ with inward flow of thermal energy, giving the low conducted heat loads characteristic of high- Z shutdowns, but with the longer CQ and low induced vessel forces characteristic of lower- Z shutdowns, as predicted by magnetohydrodynamic (MHD) simulations [13].

A central challenge of the DSP shutdown method is the shell design. Previous attempts to demonstrate the DSP technique used polystyrene shells, which were

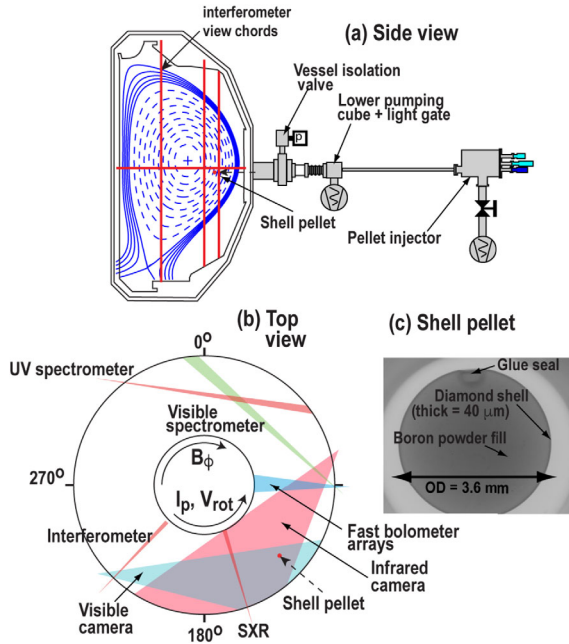


FIG. 1. (a) Schematic of pellet injector also showing equilibrium flux surfaces of target plasma; (b) tokamak top view showing key diagnostics; and (c) x-ray image of shell pellet.

unsuccessful, either not burning through in the core (for thick-walled shells) or breaking during launch (for thin-walled shells) [14]. Here, the first successful demonstration of DSP shutdown with core impurity dispersal is presented, which is achieved by the use of diamond shells.

Experimental technique.—The experiments were performed on the DIII-D tokamak [15]. Medium-energy ($W_{th} \approx 0.8$ MJ) deuterium H-mode lower-single null plasmas were used. Figure 1(a) shows a schematic of the pellet launcher. The pellets are launched using helium propellant, which is then removed by two pumping ports. Initial pellet velocities of 80–250 m/s are measured with a light gate. Additional essential diagnostics, shown in Fig. 1(b), include spectrometers, a visible fast-framing camera, an infrared camera, a CO₂ interferometer, and photodiode arrays to measure the total and soft x-ray (SXR) brightness. The shell pellets used here had 3.6 mm outer diameter and a 40 μm wall thickness. The wall was made of chemical vapor deposited diamond. The payload was 21 mg of boron dust with a 44 μm maximum outer diameter (OD).

Demonstration of shell pellet shutdown.—The main diagnostic used was the visible camera, which was operated with either B-II 412 nm (5 nm bandpass) or C-II 514 nm (4 nm bandpass) interference filters. Figures 2(a)–2(h) show visible images (with the B-II filter) at different time steps: $t \equiv t - t_{impact}$, where t_{impact} is the time at which the first light from the pellet-plasma interaction is observed. It can be seen that the pellet trajectory is fairly close (within ~ 1 cm) of the expected straight-line vacuum trajectory (dashed line), allowing an estimate to be made of the pellet minor radius: $\rho = r/a$; Figure 2(i). The pellet light

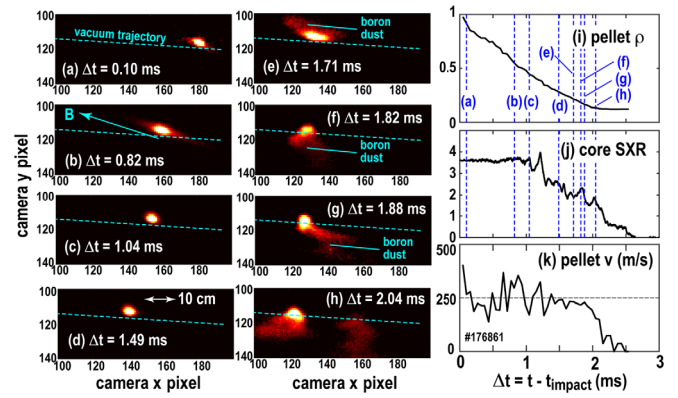


FIG. 2. (a)–(h) Visible images of shell pellet trajectory at different time steps; (i) inferred pellet minor radius; (j) core SXR brightness vs time; and (k) inferred pellet velocity.

emission can initially be seen to be fairly localized to the pellet and to be extended along B , which is the magnetic field. In Fig. 2(e), however, a cross-field dispersal of material can be seen, which is interpreted as shell burn-through and boron dust release. “Burnthrough” is used here in the sense of ionization out of the neutral state.

Figure 3 compares time traces of pellet burnthrough with modeling for a pellet with an initial velocity of ~ 230 m/s. The pellet trajectory is shown in Fig. 3(a), showing that pellet shells appear to burn through at $\rho \sim 0.25$, although pellet material goes farther, to $\rho \sim 0.15$, before stopping. Pellet brightness (integrated spatially over the image) is

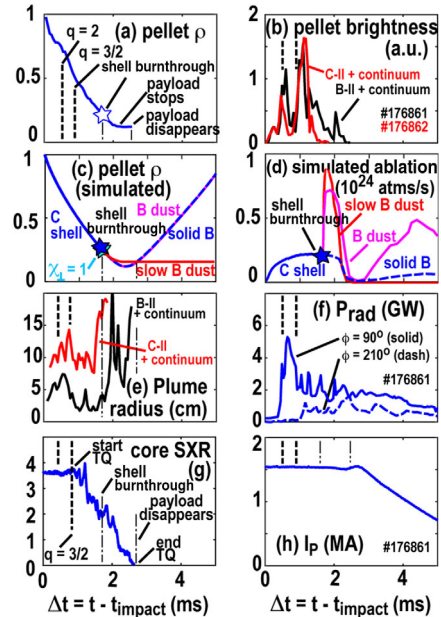


FIG. 3. Time traces of fast ($v \sim 230$ m/s) shell pellet shutdown showing (a) pellet minor radius, (b) ablation plume brightness, (c) simulated pellet minor radius, (d) simulated ablation rate, (e) ablation plume characteristic radius, (f) radiated power, (g) core SXR, and (h) plasma current.

shown in Fig. 3(b); *B*-II and *C*-II imaging (obtained from repeat shots) are similar, due to large levels of continuum emission. There are spikes in emission seen when the pellet crosses the $q = 2$ surface and again near the $q = 3/2$ surface. These spikes are not understood at present. Previous small (nondisrupting) pellets observed emission dips associated with thermal energy depletion on rational surfaces [16]. Strongly perturbing (disrupting) pellet experiments, however, exhibited emission spikes at rational surfaces, possibly from enhanced cross-field heat transport from instabilities [17]. The simulated pellet or payload trajectory is shown in Fig. 3(c), predicting shell burn-through around $\rho \sim 0.3$. For this simulation, recent calculations for carbon and boron ablation rates are used [18]. Ablated material is assumed to be deposited on flux surfaces over the width of the pellet diameter, and the resulting plasma cooling due to ionization, dilution, and radiation is calculated from CREVIN [19]. The effect of cross-field heat transport is checked using a new kinetic model [20] but is found to be small; for example, in the simulation of Fig. 3(c), including a radial thermal diffusivity of $\chi_{\perp} = 1 \text{ m}^2/\text{s}$ only increases the shell penetration depth by $\Delta\rho = 0.015$. After shell burn-through, the payload ablation is calculated in two limits: a solid boron limit, in which the boron dust is treated as a single solid pellet of equivalent mass; and an isolated dust limit, in which dust ablation is calculated as if every grain were exposed to the full plasma heat flux. As expected, *B* dust has a higher ablation rate [Fig. 3(d)], but both *B* dust and solid *B* pass through the plasma without burning through. Within the scatter of the data [Fig. 2(k)], shell pellet slowing is not observed, and is therefore ignored. *B* dust slowing is observed, however; to match this, the ablation pressure gradient force on the dust needs to be increased by 3 times [Fig. 3(c)]. This factor of 3 is not understood at present, but it could be due to interactions between dust grains, from ion drag, or from electric field forces. The disappearance in the dust signal at $\Delta t \sim 2.5 \text{ ms}$ is thought to occur because the TQ comes to an end [Fig. 3(g)], reducing ablation. Experiments using solid plastic pellets of similar radius show that solid pellets of approximately millimeter size can be observed even during the CQ, but it is likely that $<40 \mu\text{m}$ dust is not visible.

The plume radius is shown in Fig. 3(e). It can be seen that the plume is initially broader in *C*-II, which is consistent with line emission becoming dominant (relative to continuum) at the ablation plume edge. There is a rapid jump in plume radius that coincides with the observation of shell burn-through (dot-dashed vertical lines), suggesting that this jump is due to dust dispersal. Total radiated power measured at toroidal angles of $\phi = 90^\circ$ and $\phi = 210^\circ$ are shown in Fig. 3(f). It can be seen that the radiated power is asymmetric toroidally. Figure 3(g) shows the core SXR brightness, and Fig. 3(h) shows the plasma current. It can be seen that the TQ begins after the pellet crosses the

$q = 3/2$ surface, and payload dispersal then occurs roughly in the middle of the TQ.

Confirmation of boron dispersal in the plasma during the TQ is obtained spectroscopically. Figure 4(a) shows time traces of the plasma current for three shots—red curves are boron-filled shell pellet shots with $v \sim 100 \text{ m/s}$ and $v \sim 230 \text{ m/s}$, whereas the black curve is a $v \sim 100 \text{ m/s}$ tungsten powder-filled shell pellet. The core boron line emission rises before the CQ onset for the boron-filled pellets [Fig. 4(b)], which is consistent with boron being released during the TQ. Figure 4(c) shows the total plasma electron number reconstructed from interferometers for the fast boron-filled pellet shot. The upper dashed curve shows the electron number simulated from zero-dimensional (0D) ionization-recombination modeling of the injected atoms (KPRAD) [21]. Individual contributions from *C* and *B* are shown by lower dashed curves. It can be seen that the predicted total electron number is about 2 times higher than measured, possibly indicating that some of the boron persists in dust form during the CQ in the experiment, although toroidal asymmetries could also cause this. Figure 4(d) shows the mean charge states of *B* and *C* predicted by the 0D modeling. It can be seen that fully stripped ions are predicted during the TQ, with the mean charge state dropping during the CQ. Figure 4(a) also shows the simulated plasma current (from KPRAD) with and without the *B* payload included. Although these simulations are not expected to capture the precise details of the CQ (because the current profile evolution is not included), the approximate CQ duration with the *B* payload is much closer to the data than without the *B* payload, supporting a strong effect on CQ dynamics by the payload.

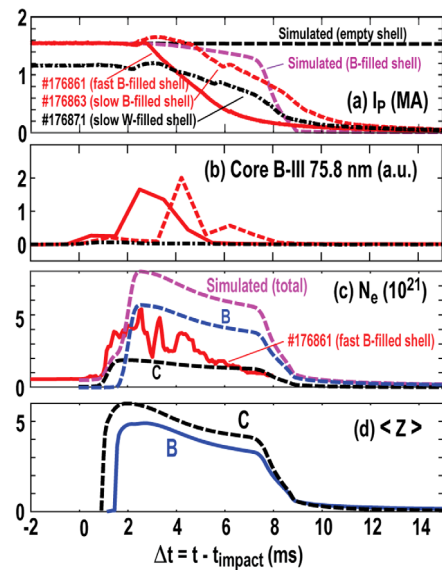


FIG. 4. Time traces of (a) plasma current, (b) core *B*-III line brightness, (c) total electron number for fast pellet with boron payload, and (d) mean charge state from 0D model.

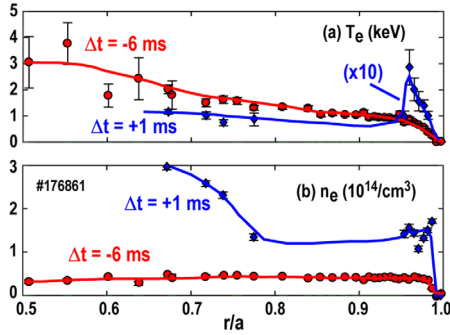


FIG. 5. Radial profiles of (a) electron temperature (with blue curve scaled times 10) and (b) electron density measured before and after pellet impact.

Some preliminary evidence of an inside-out TQ forming during DSP shutdown was obtained from Thomson scattering data, shown in Fig. 5. In Fig. 5(a), it can be seen that the temperature profile is hollow at a time of $\Delta t = +1$ ms. Because of significant jitter (on the order of 1 ms) in the shell pellet arrival time, only this isolated example of a TQ T_e profile was obtained. Additionally, the time of $\Delta t = +1$ ms is slightly prior to shell burnthrough, and so the hollowing does not appear to be due to the payload dispersal. However, these data do demonstrate that inside-out T_e profiles are achievable, and they can hopefully be made even more hollow (deeper) with less perturbing shells.

Global characteristics.—An overview of the typical disruption mitigation metrics is shown in Fig. 6 as a function of the initial pellet velocity. Figure 6(a) shows the height of the CQ I_P spike, which is interpreted qualitatively as the degree of current flattening that occurs

at CQ onset, and it is therefore inversely linked to the level of TQ MHD. A low I_P spike is desirable because it indicates low MHD mixing of impurities and is associated with better impurity assimilation. CQ duration is shown in Fig. 6(b)—it can be seen that there is a clear decreasing trend in CQ duration with pellet velocity. This trend is undesirable because it is desired to achieve long CQ duration with good heat load mitigation. Inner divertor leg heat fluence, from IR thermography, is shown in Fig. 6(c); this gives a qualitative picture of the degree of conducted heat load mitigation, showing excellent heat load mitigation (comparable to neon SPI). The integrated halo current amplitude is shown in Fig. 6(d); this gives a rough picture of the level of (undesirable) halo current vessel forces. Integrated CQ hard x-ray (HXR) signals are shown in Fig. 6(e); these reflect the level of (undesirable) runaway electron generation during the shutdown. Surprisingly, the DSP shutdowns can form REs, even with low- Z injection, indicating very rapid cooling on good flux surfaces. The colored bands in Figs. 6(a)–6(e) show approximate equivalent values for shutdowns with Ar PI, Ne SPI, and D_2 SPI. These are not for the same target plasma, being taken on different run days, and so are intended for rough comparison only. Figure 6(f) shows the estimated shell burnthrough radius as a function of initial pellet velocity.

Summary and conclusion.—This work presents the first demonstration of the shell pellet concept for tokamak disruption mitigation. This differs significantly from conventional disruption mitigation, in which impurities are dominantly mixed into the plasma by MHD processes. Many encouraging features were observed, including the core release of boron dust and evidence for rapid slowing of the dust payload after being released. Shell burnthrough appears to occur close to the minor radius predicted by ablation modeling. Assimilation of injected material (shell + payload) appeared to be quite good ($>50\%$). Low conducted heat loads, low I_P spike, and low halo currents were observed at higher pellet velocities. Undesirable trends included strong plasma perturbation by the shell (indicating a need for even lower Z shells), toroidally localized TQ radiation, short CQ duration, and RE formation. Overall, the disruption mitigation characteristics of these prototype shell pellets are quite good, giving reason to believe that even better results can be obtained with future, more optimized designs. Preliminary modeling work [18] indicates that the shell pellet concept is reactor relevant. Different shell pellets would need to be available, depending on disrupting plasma conditions. As an example, penetration to the core ($r/a < 0.4$) of a full-power ITER plasma appears to be achievable with an OD = 1.5 cm Be pellet with an experimentally achievable velocity ($v = 600$ m/s). Future experiment-modeling comparisons will hopefully strengthen these preliminary findings.

DIII-D data shown in this Letter can be obtained in digital format by following the link in Ref. [22].

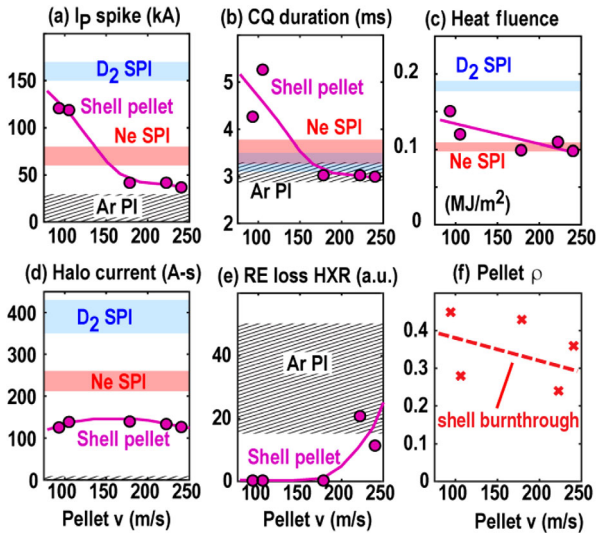


FIG. 6. Disruption mitigation metrics as a function of pellet initial velocity showing (a) I_P spike height, (b) CQ duration, (c) inner strike point conducted heat fluence, (d) integrated halo current amplitude, (e) runaway electron prompt loss level, and (f) shell burnthrough radius.

The authors wish to thank L. Chousal, J. Kulchar, A. Horton, and D. Ayala for assistance with design, testing, and installation of the pellet injector and J. Herfindal, A. Lvovsky, I. Bykov, M. van Zeeland, F. Glass, Y. Zhu, and D. Thomas for diagnostic support and A. Hyatt and H. Torreblanca for operations support. This work was supported by the U.S. Department of Energy under Grants No. DE-FG02-07ER54917, No. DE-FC02-04ER54698, and No. DE-AC05-00OR22725. This Letter was prepared as an account of work sponsored by an agency of the U.S. Government. Neither the U.S. Government nor any agency thereof, nor any of their employees, makes any warranty, express or implied, or assumes any legal liability or responsibility for the accuracy, completeness, or usefulness of any information, apparatus, product, or process disclosed, or represents that its use would not infringe privately owned rights.

-
- [1] M. G. Su, Q. Min, S. Q. Cao, D. X. Sun, P. Hayden, G. O'Sullivan, and C. Z. Dong, *Sci. Rep.* **7**, 45212 (2017).
- [2] M. D. Campbell-Brown and D. Koschny, *Astron. Astrophys.* **418**, 751 (2004).
- [3] R. P. Drake, *High Energy Density Physics* (Springer, New York, 2006).
- [4] E. Schena, P. Saccomandi, and Y. Fong, *J. Funct. Biomater.* **8**, 19 (2017).
- [5] J. A. Snipes, S. Bremond, D. J. Campbell *et al.*, *Fusion Eng. Des.* **89**, 507 (2014).
- [6] D. Humphreys, G. Ambrosio, P. de Vries *et al.*, *Phys. Plasmas* **22**, 021806 (2015).
- [7] E. M. Hollmann, G. Arnoux, N. Commaux *et al.*, *J. Nucl. Mater.* **415**, S27 (2011).
- [8] M. Lehnen, K. Aleynikova, P. B. Aleynikov *et al.*, *J. Nucl. Mater.* **463**, 39 (2015).
- [9] E. M. Hollmann, P. B. Aleynikov, T. Fulop *et al.*, *Phys. Plasmas* **22**, 021802 (2015).
- [10] N. Commaux, D. Shiraki, L. R. Baylor *et al.*, *Nucl. Fusion* **56**, 046007 (2016).
- [11] E. M. Hollmann, A. N. James, P. B. Parks *et al.*, *AIP Conf. Proc.* **1161**, 65 (2009).
- [12] P. B. Parks, Dust ball pellets for disruption mitigation, Invention Disclosure DOE Case No. S-113-472 (2007).
- [13] V. A. Izzo and P. B. Parks, *Phys. Plasmas* **24**, 060705 (2017).
- [14] E. M. Hollmann, N. Commaux, N. W. Eidietis *et al.*, *Phys. Plasmas* **17**, 056117 (2010).
- [15] J. L. Luxon, *Nucl. Fusion* **42**, 614 (2002).
- [16] W. A. Houlberg, S. L. Milora, and S. E. Attenberger, *Nucl. Fusion* **28**, 595 (1988).
- [17] E. M. Hollmann, N. Commaux, R. A. Moyer *et al.*, *Nucl. Fusion* **57**, 016008 (2017).
- [18] P. A. Parks, *Phys. Plasmas* (to be published).
- [19] H. A. Scott, *J. Quant. Spectrosc. Radiat. Transfer* **71**, 689 (2001).
- [20] P. A. Parks and E. M. Hollmann, *Phys. Plasmas* (to be published).
- [21] E. M. Hollmann, P. B. Parks, and H. A. Scott, *Contrib. Plasma Phys.* **48**, 260 (2008).
- [22] See https://fusion.gat.com/global/D3D_DMP.